THE ASTROPHYSICAL JOURNAL, 330:130–141, 1988 July 1

X-RAY OBSERVATIONS OF THE GALACTIC CENTER BY SPARTAN 1

N. KAWAI, E. E. FENIMORE, AND J. MIDDLEDITCH
Earth and Space Sciences Division, Los Alamos National Laboratory, University of California
R. G. CRUDDACE, G. G. FRITZ, AND W. A. SNYDER
E.O. Hulburt Center for Space Research, Naval Research Laboratory
AND
M. P. ULMER
Department of Physics and Astronomy, Northwestern University
Received 1987 July 27; accepted 1987 December 18

ABSTRACT

We present the results of X-ray observations of the region within 1°.25 of the Galactic center. The observations were made by the Spartan-1 free-flying Shuttle payload. Four strong, hard X-ray point sources were detected: A1742−294; 1E 1740.7−2942; 1E 1743.1−2843; and a new source SP 1744.2−2959, ~0°.5 southeast of A1742−294, which was not seen by the *Einstein Observatory*. The new source, SP 1744.2−2959, had an intensity ~20% of that of A1742−294 (2–10 keV), and was relatively hard, having spectral parameters close to those of the diffuse source and of the Galactic bulge source, GX 3+1. SPARTAN 1 did not detect the relatively strong X-ray point source seen by *Einstein* within an arc minute of the Galactic nucleus (Sgr A West), setting a 3 σ upper limit of ~1 UFU (2–10 keV). On the basis of the count rates relative to those of IE 1743.1−2843, the Galactic nucleus X-ray source appears to have been a factor of 4 fainter during the 1985 Spartan 1 observations than during the 1979 *Einstein* observations. However, we did detect hard, diffuse X-ray emission centered near the Galactic center, ~1° in extent, aligned to within 20° of the Galactic equator, and having a maximum 2–10 keV brightness of 1.5×10^{-6} ergs cm^{-2} s^{-1} sr^{-1}. In addition, we detected two weaker point sources ~0°.1 northeast and southeast of the Galactic nucleus, (GC NE and GC SE), embedded in the diffuse emission. GC SE was distinctly softer than the other sources detected. Finally, we detected a relatively uniform, diffuse emission of intensity ~2×10^{-7} ergs cm^{-2} s^{-1} sr^{-1} (2–10 keV), similar to the Galactic ridge observed by *HEAO 1*, *EXOSAT*, and *Tenma*. The spectrum of this diffuse emission shows an order of magnitude less interstellar absorption than the other Galactic center sources, suggesting a closer origin.

Subject headings: galaxies: The Galaxy — galaxies: nuclei — X-rays: sources

I. INTRODUCTION

There have been many attempts to observe the Galactic center in the X-ray band, since this is one of the few windows available for observations through the spiral arms of the Galaxy. Unlike radio and infrared images, however, X-ray images (above ~3 keV) have not revealed a clear picture of the sky within 1° of the Galactic center, partly due to the difficulty in achieving high spatial resolution, and partly due to the time variability of the sources.

The *Uhuru* satellite detected the Galactic center first but was unable to distinguish whether it was an extended source or group of point sources (Kellogg *et al.* 1971). Later, the *Ariel 5* satellite detected a transient source, A1742−289, whose error circle (radius 1°.2 contained the Galactic nucleus in Sgr A West (Eyles, Skinner, and Willmore 1975; Branduardi *et al.* 1976). *Ariel 5* also discovered the X-ray source A1742−294 ("GCX"), which is the only persistent source seen in all subsequent observations. Its location was determined by rotation modulation collimators (RMC) on both *SAS 3* (Jernigan *et al.* 1978) and *Ariel 5* (Wilson *et al.* 1977; Proctor, Skinner, and Willmore 1978). In addition, *SAS 3* discovered three X-ray bursters in this region (Lewin *et al.* 1976). In 1978 two rocket experiments performed X-ray imaging of the Galactic center with higher spatial resolution (Cruddace *et al.* 1978; Proctor, Skinner and Willmore 1978). While each experiment detected at least five point sources, only two sources, A1742−294 and GX 0.2−0.2, were positively identified by both experiments. The *Einstein* observations made in 1979 achieved both better spatial resolution and greater sensitivity (Watson *et al.* 1981), so that in the 1° × 1° field of view of the IPC, a dozen point sources were detected with a spatial resolution of 1′, including A1742−294 at the edge of the field of view. Two important discoveries emerging from the *Einstein* observations were the detection of a hard point source, 1E 1742.5−2859, located within 1′ of the nucleus, and diffuse X-ray emission distributed asymmetrically around the Galactic center. The energy spectrum of 1E 1742.5−2859 was consistent with a thermal spectrum with $kT \approx 5$ keV and $N_H \approx 6 \times 10^{22}$ cm^2, and the luminosity was 1.5×10^{35} ergs s^{-1} (0.5–4.5 KeV). The diffuse emission had a similar spectrum with a total luminosity in the energy range 0.9–4.0 keV of 2.2×10^{36} ergs s^{-1}. The *Einstein* Galactic Plane Survey conducted by Hertz and Grindlay (1984) revealed one more source in the region of interest, 1E 1740.7−2942, with a statistical significance of 5 σ.

So far, only the *Einstein Observatory* has had the sensitivity and angular resolution necessary to image the small, crowded region of the X-ray sky near the Galactic center, but it had limited spectral resolution in a narrow band of energies (0.5–3 keV). Here we present observations of the Galactic center made from Spartan 1, which achieved both arcminute spatial resolution and a modest degree of spectral resolution over a relatively broad band of X-ray energy (1–15 keV). Spartan 1 detected six point sources in the region within 1° of the Galactic center but unlike *Einstein* (Watson *et al.* 1981), did not detect a point X-ray source near the nucleus in Sgr A West. Moreover, a diffuse source around Sgr A West was discovered having an intensity comparable to, but larger in extent than, that measured by *Einstein*. There is also evidence for a more global diffuse emission which could be related to the emission from the Galactic ridge reported by *EXOSAT* and *Tenma* (Warwick *et al.* 1985; Koyama *et al.* 1986). Our observations were made on 1985 June 20–21 UT. Six weeks later, a *Spacelab* experiment viewed this same region and obtained similar results (Skinner *et al.* 1987).

This paper is organized as follows: In the following section (§ II) we present the observational details. Section III*a* briefly describes the spatial analysis of the sources, including the Maximum Entropy Method (MEM) in § III*a*(i), and a linear fitting technique in § III*a*(ii). Section III*b* discusses the spectral fitting, while §§ III*c*(i)–III*c*(v) describe the characteristics of the individual sources. A general discussion is given in § IV, followed by a summary in § V. A more detailed description of the MEM image production is given in the Appendix.

II. OBSERVATIONS

Spartan 1 was the first of a new class of carrier for astrophysical observations in space. Spartans are autonomous free-flying payloads released by the shuttle in Earth orbit. There they perform observations and collect data for several days and then are retrieved by the shuttle. Spartan 1 was released by the orbiter Discovery (STS mission 51-G) on 1985 June 20, and its purpose was to observe the Galactic center and the Perseus cluster of galaxies. This instrument scanned its target using narrowly collimated proportional counters with a field of view (FWHM) of 5′ × 3°, the longer dimension being perpendicular to the scanning direction. The payload contained two identical sets of proportional counters, each having an effective area of ~ 660 cm^2. Each counter contained two layers of anode wires, each layer having a depth of ~ 2.8 cm. The counters had a 2.5 μm Mylar window and were filled with P-10 gas (Ar-methane mixture) at a pressure of 1 atm; consequently they were sensitive to X-rays in the energy range 1–5 keV. A 1 UFU Crab-like source (1mCrab) would count ~ 1.9 s^{-1} in each detector in the 2–10 keV energy range. A five sided coincidence detection system was used to discriminate against particle-induced events. For more details of the Spartan 1 instrumentation, see Fritz *et al.* (1987). The observations were performed by scanning the collimator field across the Galactic center at a uniform rate of $\sim 20''$ s^{-1}.

Fourteen scans of the Galactic center were planned, with the directions of these scans distributed symmetrically about the Galactic center. Each scan comprised three colinear segments, a short segment originating at Sgr A West and of length 1°, a long segment starting at the end point of this short segment and running 2° back through Sgr A West and finally another short segment returning the X-ray axis back again to Sgr A West. As a consequence of premature depletion of attitude control gas and of automatic detector shutdown during passage through the South Atlantic Anomaly (SAA), some segments were lost. In all, 18 segments in seven different scan directions yielded useful data: 12 short segments of length 1° and 150 s exposure (~ 188 time bins per segment), five long segments of length 2° with 300 s exposure (~ 377 time bins), plus a portion ($\sim 50\%$) of one long segment, truncated at the beginning by a pass through the SAA (Fritz *et al.* 1987). Thus, a total of 7111 s of data was collected in 8657 time bins, counting the data from detectors 1 and 2 separately. As a result, the region within 1°.25 from the Galactic center was covered reasonably well by scans in a variety of directions. The region as far as 3° from the Galactic center was less well covered, and with diminished sensitivity. We detected a contribution from one source only (GX 3+1) from this outer region in a half dozen scans. Figure 1 diagrams the scan paths in relation to the sources on the MEM map (see §§ III*a*[i] and III*a*[ii]).

X-ray counts were accumulated every 0.8212 s in 128 energy bins for both layers of each detector. The energy gain of each layer was calibrated each orbit using an ^{55}Fe source. A slow drift in gain was observed during the mission (Fritz *et al.* 1987), which we have compensated for in the data analysis.

The aspect (pointing direction) of the detector was monitored at regular intervals by an optical system and was determined with an accuracy of 30″. Since the positions of the strong point sources, A1742−294 and GX 3+1, are known with better accuracy than our optical aspect solution (Proctor, Skinner and Willmore 1978; Bradt and McClintock 1983), a refined aspect solution was found for each scan by fitting the X-ray transits of these sources to their known positions. The refined positions of the scans differed from the unrefined positions by less than 72″ (the shifts had an rms of 32″ and consequently exerted only a small influence on our results).

III. ANALYSIS AND RESULTS

a) *Spatial Analysis*

Two methods were employed to analyze the spatial distribution of the X-ray sources. One was the maximum entropy method (MEM) reconstruction technique (Gull and Daniel 1978; Willingale 1981), which estimates the intensity distribution with few *a priori* assumptions. The other method fits the scan data to models containing point and diffuse sources, thus yielding more accurate estimates for the positions and intensities of sources which have been identified with confidence in the MEM image.

i) *MEM Reconstruction Imaging*

A two-dimensional image reconstruction was performed using the MEM technique for a square 2°.5 × 2°.5 field centered at the Galactic center. This field was subdivided by a 241 × 241 lattice with a 37″.5 spacing. In order to maximize the signal-to-noise ratio, data in the energy range of 2–10 keV were used. Data were taken from the upper layer of each detector only, as the bottom layer had a lower sensitivity and would have decreased the signal-to-noise ratio if used. The intrinsic detector background caused by unvetoed particle events was subtracted from the data. The background was determined by using a correlation between the detector signal counts and the coincidence count rate, which was obtained while Spartan 1 was observing source-free regions outside the galactic plane (Fritz *et al.* 1987). The count rate for the background varied from 2.7 to 3.9 counts per 0.8212 s with systematic errors less than 0.3 s^{-1}. Simulations have shown that the effect of changes in this background on the MEM map was negligible.

Although it is desirable that the MEM image reconstruction be free of *any* assumptions, some information derived by the scan-fitting technique had to be incorporated, namely, the corrections to the aspect solution and the detection of X-ray sources outside of the 2°.5 × 2°.5 field. Although GX 3+1 is 2°.4 from the Galactic center, well outside the region of interest, it contributed a considerable number of counts to the observa-

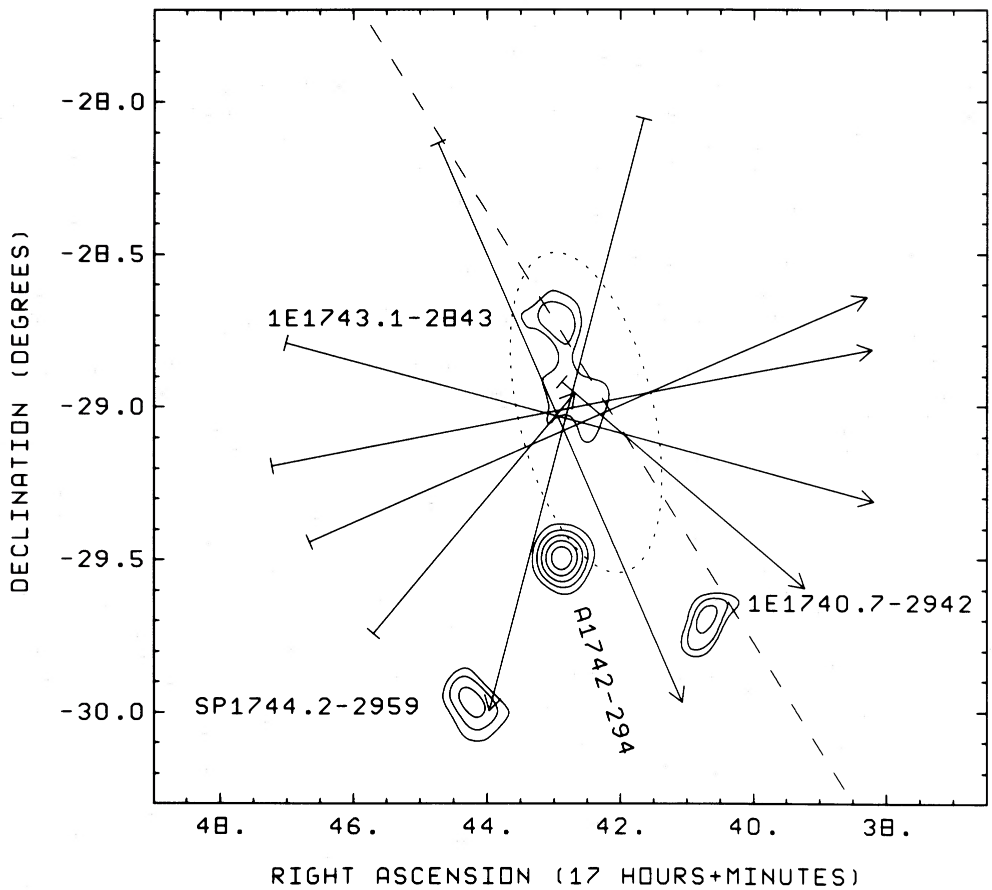

FIG. 1.—The MEM map derived for the region within 1°25 of the Galactic center (see § III*a*[i] and the Appendix) with the scanning trajectories overlaid (see § II). Four point sources (A1742−294; the new source, SP 1744.2−2959; 1E 1740.7−2942; and 1E 1743−2843) and one diffuse source covering the Galactic center are visible in this map. The dashed ellipse represents the extent of this centrally localized diffuse emission as determined by linear fitting of the data to a simplified model (see § III*a*[ii] and Table 2). The contour levels plotted range from 19637.4 to 375 counts cm^{-2} s^{-1} sr^{-1} in equal logarithmic intervals, while the dashed oblique line represents the Galactic equator.

tion due to the 3° long axis of the collimator. These counts were estimated using the results of the scan-fitting technique and then subtracted from the data. We have confidence in this scan-fitting procedure because a good value of χ^2 (8735 for 8657 data points) was obtained (see Table 1 and § III*a*[ii] which follows immediately). In addition, the linear fitting solution and the MEM map are consistent with each other (see the Appendix for a detailed description of how the MEM map was generated).

The resulting MEM map, shown in Figure 1, reveals five features within 1°25 of the Galactic center at 17^h42^m5, −28°59′. The area enclosed by the ellipse is a feature established by the source-fitting analysis, which is crudely matched by the extended diffuse region marked by the lower contours of the MEM map (not shown). Four of the features are pointlike, and one appears to have a diffuse or confused structure. The strongest source in the map, located ~0°5 south of the Galactic center, is A1742−294, which has been observed consistently in rocket and satellite observations. Two other sources may be identified with the *Einstein* sources, 1E 1743.1−2843 (Watson *et al.* 1981) in the north part of the map, and 1E 1740.7−2942 (Hertz and Grindlay 1984) in the southwest.

However, in the region within about 15′ of Sgr A West, shown in the enlargement of the MEM image given in Figure 2, there is little similarity between the Spartan 1 and *Einstein* observations (the *Einstein* source locations are given by arabic numbers). We did not observe a *prominent* source near the nucleus[1], whereas *Einstein* detected a source yielding about twice the IPC count rate of the northern source, 1E 1743.1−2843 (source 10; Watson *et al.* 1981). Instead we observed weak X-ray emission which may be diffuse or a confusion of several point sources (see §§ III*c*[v] and IV*c*). We can rule out the possibility of nearby strong sources masking a weak point source in this region, since the two long scans which cross the galactic center in a southerly direction (see Fig. 1) "see" no other strong sources during their passage. Apart from sources 6 and 10, there is no positive evidence for the other sources observed by *Einstein* (Watson *et al.* 1981), even though sources 5, 7, 9, and 11 were hard, and near the threshold of our sensitivity (~3×10^{34} ergs s^{-1} in Watson *et al.* 1981, or ~10^{36} ergs s^{-1} in Table 2). In particular, a prominent

[1] Although the preliminary (higher entropy) MEM maps derived without using the iterations of eq. (1) in the Appendix do show a more prominent feature centered between Sgr A West and source 2 of Watson *et al.* (1981), these maps cannot be justified because of their large χ^2. Moreover, in the scan-fitting model described below, a point source which was *initially* located at Sgr A West converged to the position of the weak point source, GC SE, during the iterations. Further reduction of the MEM map χ^2 below the value used for Figs 1 and 2 gradually changed the local maximum near Sgr A West into a ridge distinctly separated from Sgr A West (see the Appendix).

feature appears in the *Einstein* MEM-processed image (Fig 2*c* of Watson *et al.* 1981), which was interpreted as two sources, 11 and 12, whose combined IPC count rate was 12.4 s^{-1}, slightly less than that of 1E 1743.1−2843 (source 10, 16.1 counts s^{-1}). This feature is absent from the Spartan 1 image (Fig. 2).

The point source in the southeast portion of the map (Fig. 1) has not been reported before but was observed by Spacelab 2 about 6 weeks after the flight of Spartan 1 (Skinner *et al.* 1987). We find no evidence from the MEM map for the other *point sources* reported in earlier observations such as GX 0.2−0.2 (Cruddace *et al.* 1978; Proctor, Skinner, and Willmore 1978) and A1742−289 (Eyles, Skinner, and Willmore 1975; Branduardi *et al.* 1976) at $17^h43^m55^s$, $-28° 52'33''$ and $17^h42^m26^s$, $-28°59'.8$, respectively, even though we would have detected both easily.

It is difficult to quantify the uncertainties in the intensities and locations of the sources due to the nonlinearity inherent in the MEM process. The net result is that the MEM map intensity of a relatively weak source is influenced by its proximity to strong sources. Thus, other, linear fitting techniques must be used to *measure* the locations, intensities, and spectra of the individual sources. (However, the MEM map and linear fitting agree on the location and mean surface brightness of the diffuse source—see § III*c*[v].

ii) *Model Fitting*

Having initially determined the point source distribution on the MEM map, we then fitted the X-ray count history of the scanning data to models using the same data set as before, namely the X-ray counts from the upper layer of each detector in the energy range 2–10 keV, with the background estimated from the coincidence counts. The uniform X-ray background was negligible.

We tested models of the X-ray intensity distribution consisting of several point sources, a uniform background, and in some cases, a simple model of diffuse emission at the galactic center. The four point sources evident in the MEM map and GX 3+1 were included in every model, and additional point sources were introduced to improve the fit. A uniform back-

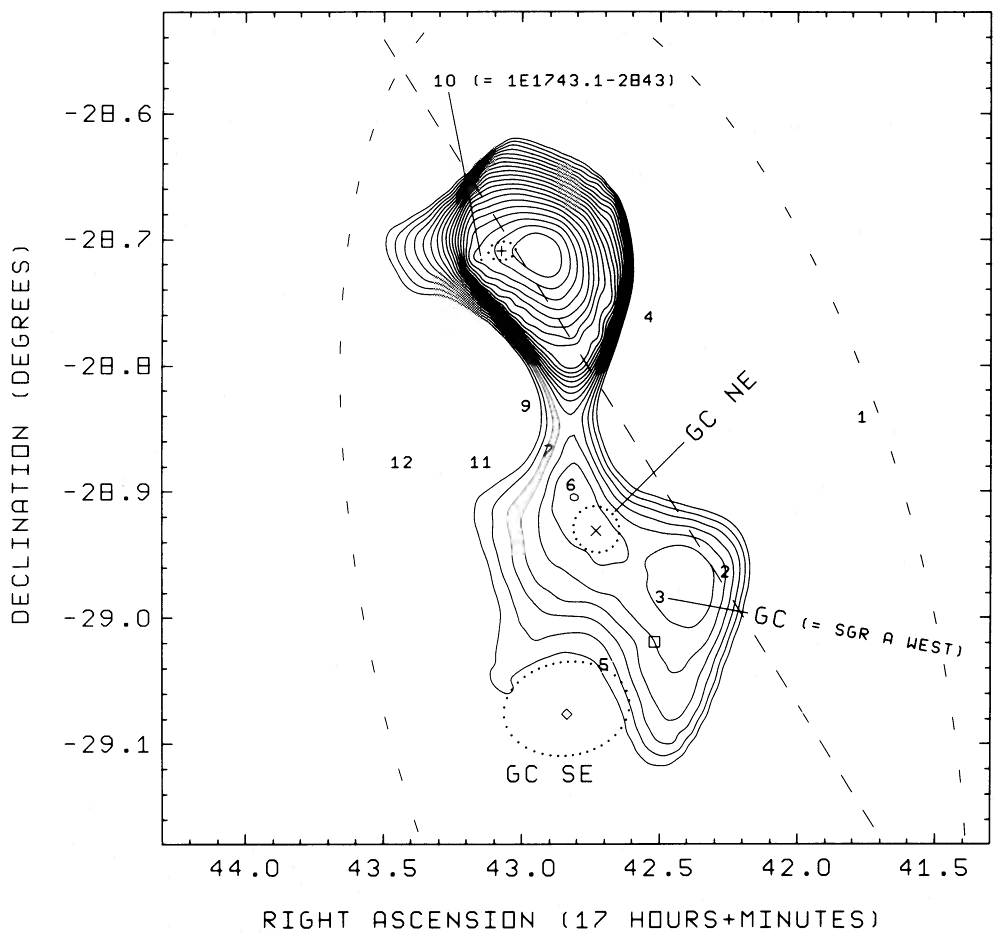

FIG. 2.—The MEM map near the Galactic center. The dashed ellipse and oblique line represent the diffuse emission determined by linear fitting and the Galactic equator, respectively, as in Fig. 1. The contours range from 2009.4 to 375.0 counts cm^{-2} s^{-1} sr^{-1} in uniform logarithmic intervals. The numbers represent the locations of the sources from Table 2 of Watson *et al.* (1981), with the Sgr A West location marked as source 3 (see § IV*a*). The position of source 10 from Watson *et al.* is marked by the dot, just to the left of the plus sign and dotted ellipse (the 90% contour for the position of 1E 1743.1−2843 derived from the linear fitting—see § III*c*[iii] and Table 2). The 90% contour for the GC NE source (see Table 2) is marked by the circle of dots around the cross (see § III*c*[iv]), while the dotted ellipse marks the 90% contours for the GC SE source, with the diamond marking the best-fit position. The square marks the center of the centrally localized diffuse emission determined by the linear fitting (the 90% contour for this center is an ellipse similar to the large [1 σ] ellipse, but only ~400″ in size, and is not shown in this figure). The open circle below source 6 is part of the 637.2 counts cm^{-2} s^{-1} sr^{-1} contour (see § III*c*[iv]).

ground was also included as a free parameter in all models to describe the offset due to the diffuse X-ray emission from the Galactic ridge emission. When the centrally localized diffuse emission was included, it was modeled by a two-dimensional elliptical Gaussian distribution, where the length of the major axis, the ellipticity, the inclination of the major axis on the sky, the integrated intensity and the position of the center of the distribution were free parameters. The positions of the point sources other than A1742−294 and GX 3+1 were allowed to vary to find the best fit solutions, and the intensities of all sources were free parameters. The models tested and the χ^2 for the best fits are summarized in Table 1.

Table 1 shows that χ^2 decreases by almost 200 when the seventh and eighth point source of model 3 are replaced by a diffuse emission component in model 4, both models having the same number of free parameters (39). In order to compare the quality of this fit of models with different numbers of free parameters, we used an *F*-test (see, e.g., Press *et al.* 1986). Adding one more point source to model 4 decreases χ^2 by 20.3, which justifies the extra three parameters in model 5 with greater than 99.9% confidence. Model 5 can be shown to be superior to models 1–3 in a similar fashion. On the other hand, adding another point source to model 5 corresponds to a statistical confidence of only 86% for model 6, which, therefore, is not well justified. In most of the models which included more point sources than A1742−294, GX 3+1, SP 1744.2−2959, 1E 1740.7−2942, and 1E 1743.1−2843, a point source was initially located at the position of Sgr A West. *In none of these cases did this* point *source remain at that position during the fitting iterations* (*see below*). In adddition, some models with many point sources had two of the sources initially located at 1E 1743.1−2843 and at the maximum in the MEM map located a few arc minutes to the west (see Fig. 2). In all of these cases, only 1E 1743.1−2843 remained as a viable point source.

Thus model 5, having seven point sources (counting GX 3+1) a uniform background, and the centrally localized diffuse emission fits the data best (see Fig. 2). The best fit contained two sources: GC NE and GC SE (which was absent on the MEM map). These sources are located ~0°.1 from the Galactic center and embedded in the diffuse feature on the MEM map (Fig. 2). The best fit χ^2 is 8735 for 8615 degrees of freedom, where no systematic effect (such as source variability or the uncertain long axis response of the collimator) other than scan shifts has been taken into account. Although this value of χ^2 (reduced $\chi^2 = 1.014$) is still unacceptable on purely statistical grounds with more than 99% confidence, we consider it to be an excellent fit considering all the possible systematic effects and the simplicity of the diffuse source model.

The 90% confidence contour levels of the resultant positions of the point sources are shown for the weaker sources in the expanded map (Fig. 2), and the extent of the Gaussian intensity distribution of the centrally localized diffuse emission is shown in Figures 1 and 2. The contours for the point sources represent statistical confidence limits that should be treated with some caution because of the "poor" χ^2, whereas the contour for the diffuse emission describes the location where the surface intensity is $e^{1/2}$ times that of the center. The position, 90% confidence error radius, and intensity of each source are also listed in Table 2. The intensity of the uniform background, which is not listed in Table 2, is 4.2 ± 0.2 counts s^{-1} deg^{-2}, or 21 ± 1 counts s^{-1} cm^{-2} sr^{-1}. The $e^{-1/2}$ semimajor axis of the central diffuse emission is 0°.54 ± 0°.05, the ratio of the minor to the major axis is 0.41 ± 0.05, and the angle of the major axis from the Galactic plane is 18° ± 5°.

TABLE 1

MODELS OF SPATIAL FIT

Model	Point Sources	Central Diffuse	Number of Parameters	Degrees of Freedom	χ^2	Reduced χ^2
1......	6	No	33	8624	9087.	1.054
2......	7	No	36	8621	8965.	1.040
3......	8	No	39	8618	8944.	1.038
4......	6	Yes	39	8618	8756.	1.016
5......	7	Yes	42	8615	8735.	1.014
6......	8	Yes	45	8612	8730.	1.014

b) *Spectral Analysis*

The spectra of the sources were analyzed using only data obtained from the upper layer of the detectors. The data in the observed energy range (0.7–11.4 keV for detector 1, and 0.9–13.7 keV for detector 2) were divided into 12 spectral bands, and then each data set was fitted as before. However, in this calculation we fixed the X-ray source positions and the parameters of the diffuse source at the values obtained by fitting the 2–10 keV data, leaving only intensities as free parameters. In addition, the data from the two detectors were fit separately, thus providing two sets of 12-channel spectral data for each X-ray source, including the uniform background. No systematic errors were considered, and all the uncertainties of the spectral parameters were derived from the Poisson statistics of the original data.

The pulse-height spectrum of each source was fitted to a power-law model and a thermal bremsstrahlung model, both containing a factor describing interstellar absorption. The resulting values of χ^2 and the best-fit parameters are summarized in Table 2. In addition, the luminosity of each source, based on the best-fitting thermal bremsstrahlung model, is listed. Both models were unacceptable for the brightest source, A1742−294, and the uniform background. The spectrum of the weakest point source, GC SE, can be fit by a thermal bremsstrahlung model only. The other sources have spectra consistent with both power-law and thermal bremsstrahlung models. The absorption column density derived from the fitting varies from source to source. With the exception of the uniform background only, every source shows a relatively high absorption column density consistent with, or greater than, the interstellar absorption expected for an X-ray source located at the galactic center. The 68% χ^2 contours in the $KT - N_H$ plane of the thermal bremsstrahlung model are shown for all sources in Figure 3.

c) *Results for Individual Sources*

i) *A1742−294*

A1742−294 was the strongest source in our observations. Its signal, clearly visible in the raw data, is highly variable (see § III*d*). We find that neither the thermal bremsstrahlung model nor the power-law model fits the spectrum when no systematic error is considered. According to recent studies of X-ray spectra, simple models, such as those we employed, cannot generally describe the spectra of low-mass binary systems (Mitsuda *et al.* 1984; for a theoretical study see Czerny, Czerny, and Grindlay 1986) and massive systems (White, Swank, and Holt 1983). Thus, it is not surprising that we do not obtain a good fit for an X-ray source with good photon statistics.

TABLE 2

X-Ray Sources Detected in SPARTAN Observations

Parameter	A1742−294	GX 3+1	SP 1744.2−2959	1E 1740.7−2942	1E 1743.1−2843	GC NE	GC SE	Diffuse[a]
Position (1950.0):								
R.A.	265.7217	266.2046	266.0534	265.1724	265.7688	265.6830	265.7093	265.7093[b]
Decl.	29.4936	−26.5472	−29.9813	−29.7225	−28.7098	−28.9312	−29.0765	−29.0192[b]
90% error radius	(fixed)	(fixed)	16″	22″	32″	66″	160″	400″
2–10 keV counts s^{-1}[c]	43.71	44.4	10.88	7.58	4.66	2.38	1.16	17.9
1 σ	0.42	2.5	0.32	0.26	0.29	0.26	0.23	1.6
Spectral fit:								
Thermal bremsstrahlung:								
χ^2	50.6	22.4	13.8	13.4	17.5	11.9	8.7	13.1
Reduced χ^2	2.61	1.06	0.70	0.66	0.62	0.83	0.57	0.41
kT (keV)	5.1	5.6	4.4	14.3				
1 σ	0.3	+3.2/−1.3	+1.2/−0.8	+15.3/−5.4	11.2	10.0	0.5	21.3
log N_H (cm^{-3})	22.913	22.586	22.756	23.162	+43.7/−5.7	+14.0/−6.3	+0.9/−0.4	+300/−14
1 σ	0.15	0.10	0.055	0.073	23.29	22.59	23.46	22.61
X-ray flux (10^{-11} ergs s^{-1}					0.18	0.22	0.35	0.17
cm^{-2})	110	76	20	25	19	4	73	34
luminosity at 10 kpc (10^{35}								
ergs s^{-1})	130	9	24	30	23	5	87	41
Power-law:								
χ^2	48.83	22.55	11.97	13.01	17.66	11.76	>32	12.97
Reduced χ^2	5.62	2.33	1.07	0.5	0.84	0.56	...	0.62
Photon index	2.80	2.49	2.86	2.00	2.2	2.2	...	1.8
1 σ	0.08	0.42	0.30	0.35	0.8	0.9	...	0.6
log N_H(cm^{-3})	23.003	22.670	22.857	23.206	23.37	22.72	...	22.70
1 σ	0.016	0.11	0.062	0.085	0.21	0.25	...	0.20

[a] Centrally localized diffuse component.

[b] Position of the center of the Gaussian distribution of X-ray brightness.

[c] Count rate for one counter with an effective area of 660 cm^{-2}.

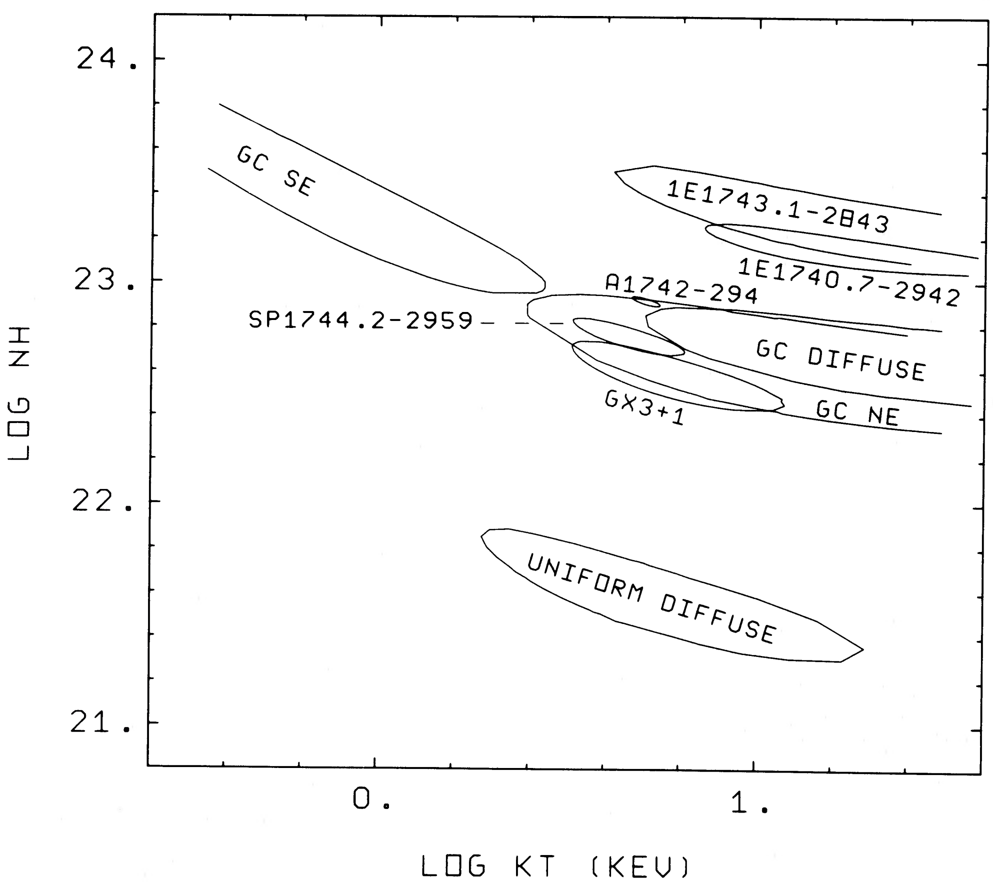

Fig. 3.—The 68% χ^2 contours for the fits of a thermal bremsstrahlung model applied to the Galactic center sources (see Table 2 and § III*b*). The areas enclosed by the contours vary inversely with the strength of the source. A dashed line indicates the error contour of the new source, SP 1744.2−2959.

Nevertheless, we use the nominal best-fit parameters to characterize the spectrum of A1742−294, because they contain sufficient information to compare it with the other observed X-ray sources, whose spectral parameters are less well determined. The nominal best-fit spectral parameters are similar to those of GX 3+1 (Fig. 3). GX 3+1 is usually categorized as a bright bulge source (Bradt *et al.* 1979), and is an X-ray burster (Inove *et al.* 1981) and a QPO source (Lewin *et al.* 1986). In addition, A1742−294 was observed to vary by at least 30% over a timescale of a few seconds during a rocket observation lasting a few minutes (Cruddace *et al.* 1978) and the Spartan 1 data confirms this (§ III*d*). Thus, while A1742−294 shows strong persistent emission, it is also variable (Lewin *et al.* 1976), is probably a burster, and may be a QPO source.

ii) *The New Source, SP 1744.2−2959*

This source was discovered by the Spartan 1 experiment. Six weeks after our observation, it was also detected by Spacelab 2 (Skinner *et al* 1987). Figure 3 shows the spectral parameters of this source to be similar to those of A1742−294 and GX 3+1, and thus SP 1744.2−2959 could also be a burster or a QPO source.

iii) *1E 1743.1−2843 and 1E 1740.7−2942*

These two sources both show such high absorption (i.e., $N_H > 10^{23}$) that it is likely to be intrinsic to the sources themselves (even if these sources are being seen through the *entire* galaxy). This kind of high intrinsic absorption is often observed in X-ray sources such as GX 301−2 (e.g., White and Swank 1984; Leahy *et al.* 1987) and Vela X-1 (e.g., Ohashi *et al.* 1984) and is usually attributed to material local to the X-ray source.

The model-fitted position for 1E 1743.1−2843 is about 1′.5 west of the *Einstein* position, while the local maximum on the MEM map lies a few arc minutes farther west from the model-fitted position (Fig. 2). Since the model-fitted results indicated only one point source in this neighborhood, we believe the disagreement between the MEM and model-fitted locations to be due to the time variability of stronger sources during the relevant scans, or to the centrally localized diffuse background (which gets brighter to the west of 1E 17431−2843 according to the model-fitted results), or both. However, the local maximum is extended toward the position of the *Einstein* source (Fig. 2), with a contour bending sharply around it just before a precipitous drop in the map intensity, indicating that the MEM iterations "felt" the presence of the *Einstein* source 10, even though the bulk of the local maximum lies farther to the west.

iv) *The Two Sources 0°.1 from the Galactic Center—GC NE and GC SE*

These two sources are required by the linear technique to give a good fit, although only GC NE (near source 6 of Watson *et al.*—see Fig. 2) is visible in the MEM map. However, simulations have shown that the MEM map can lose such weak sources due to the effects of either diffuse emission or stronger nearby point sources. The two are located near Sgr A West, but the positions of both are inconsistent with Sgr A West, as can be seen in Figure 2. The source ~0°.1 southeast of Sgr A West (GC SE) has a fairly large 90% confidence region which touches 1E 1742.7−2902 (source 5 of Watson *et al.* 1981—see Fig 2), one of the weak hard sources detected by the *Einstein* observations. A distinctive feature of this source is its peculiar pulse-height spectrum, which cannot be fit by a power-law model. A successful fit is obtained using a bremsstrahlung model; the derived absorption column density is similar to that of the other sources, but the spectral temperature (~0.5 keV—see Table 2) is significantly lower. When the spectrum is corrected for the large absorption, the source luminosity is $\sim 10^{36}$ ergs s^{-1} (see Table 2) comparable to that of A1742−294 and GX 3+1. The derived spectral parameters for GC SE suggest that it belongs to the class of objects having relatively high luminosities and soft spectra, often referred to as "ultra soft sources" like GX339−4 (Makishima *et al.* 1986), which have been suggested as black hole candidates (White, Kaluzienski, and Swank 1984; White and Marshall 1984).

GC NE has spectral parameters which are identical to those of A1742−294, GX 3+1, SP 1744.2−2959, and the centrally-localized diffuse emission (see Fig. 3), with $kT \approx 10$ keV, and log $(N_H) = 22.6$ (see Table 2), which suggest that it belongs to the galactic bulge class of sources, and may be a burst or QPO source. The 90% confidence region of the model-fitted location lies on an elevated contour of the MEM map (Fig. 2), just a few arc minutes south-southeast of a small local maximum in the map and IE 1742.8−2853 (source 6 of Watson *et al.* 1981). Both the local maximum of the MEM map and the model-fitted feature (GC NE) could be consistent with 1E 1742.8−2853.

v) *The Centrally Localized Diffuse Emission*

Since the mean shape and intensity of the diffuse emission determined by the MEM map and the diffuse emission determined by the MEM map and the linear fitting agree well (see the Appendix), we will proceed to discuss the details of the diffuse emission using the simplified result derived from the linear fitting. The 90% confidence region for the center of the two-dimensional elliptical Gaussian distribution of the diffuse emission is not shown in Figure 2, but has a shape which is similar to the 1 σ ellipse with a 400″ semimajor axis (see Table 2). This confidence region includes Sgr A West and is very close to the Galactic center. The ratio of the minor to the major axis is 0.41, which is reasonably close to the 0.5 value obtained from the *Einstein* observations (Watson *et al.* 1981). The major axis of the source spans more than 1°, almost twice that of the *Einstein* observation, which extends only 0°.6 at the lowest contour (Watson *et al.* 1981). Perhaps this difference could be due to the different energy ranges of the two instruments. If so, this implies that the hard X-ray diffuse emission is more extensive. The angle of the major axis with respect to the Galactic plane is 18°, somewhat large compared to that of the *Einstein* diffuse source, which appears to be aligned parallel to the Galactic plane. The surface intensity of the source is $\approx 1.5 \times 10^{-6}$ ergs s^{-1} cm^{-2} sr^{-1} at the center (in excellent agreement with the ~200 counts cm^{-2} s^{-1} sr^{-1} mean of the MEM map in this region although we do not display the lower contours in Figs. 1 and 2), and 9×10^{-7} ergs s^{-1} cm^{-2} sr^{-1} at the $e^{-1/2}$ level of the peak. We compare this value to those of previous observations in the following section. It has a spectrum similar to A1742−294 and an absorption column density consistent with a location near the galactic center.

vi) *The Uniform Background*

We included this component in the model in order to account for any diffuse background which appeared to have a constant brightness across the map. It has a surface intensity ~20 counts s^{-1} cm^{-2} sr^{-1}, or roughly 2×10^{-7} ergs s^{-1} cm^{-2} sr^{-1}. Since its spectrum could not be fitted by thermal bremsstrahlung or power-law models, we attempted a fit using a combination of the two. The fit of the combined models is an improvement, but it is still not satisfactory. The thermal bremsstrahlung component accounts for the photons in the lower energy band, 1–5 keV, with relatively low temperature (<3 keV) and low absorption column density ($<10^{22}$—see the "uniform diffuse" confidence region in Fig. 3), whereas the power-law component with photon index ≈ 0 accounts for the photons in the higher energy range at 5–10 keV. We cannot reject the possibility that some portion of the detector background remained in the data which we processed. However, the spectrum is very different from the spectrum of the detector background which we estimated from the observation of the off-Galactic plane sky, and follows the detector efficiency more closely than the detector background. We therefore believe that most of the uniform background is X-ray emission in the line of sight to the Galactic center.

d) *Time Variability*

The plot of the difference of the count rate of the original data and the rate predicted by using the source locations and intensities of the linear fitting revealed no obvious periodic intensity modulation in the stronger sources. Because of the 0.82 s data integration time, we could not detect periods shorter than 1.64 s. Variability on a time scale shorter than the time of passage of the collimator over the point sources (~ 12 s) would tend to increase the χ^2 of a single scan of a given source. Variability on a longer time scale would tend to increase the χ^2 of several scans over a given source. No such effects were detected for any source other than A1742−294, although the corresponding limit was probably near 50% modulation for SP 1744.2−2959 and A1740.7−2942, and $\sim$100% for 1E 1743.1−2843. Approximately half of the 12 pairs of scans which passed over A1742−294 showed significant erratic variability of order 20%–100% with occasional rise times at least as short as the 0.82 s data bin time. Because of this variability, it is difficult to place limits on the bursting activity of A1742−249, although we can probably say that the source luminosity did not jump by a factor of 4 during the appropriate scan intervals.

IV. DISCUSSION

For purposes of discussion in this section, we will assume that the source locations, intensities, and spectra derived from our analysis of the data are correct.

a) *X-Ray Emission from Sgr A West*

Prior to Spartan 1, only *Einstein* had observed Srg A West as an X-ray source. The most significant difference between our results and the *Einstein* observations is that we did not detect a point source at the position of Sgr A West. There are several possible explanations. Since our observation technique is intrinsically unable to detect the time variability of an indivual source, interference from other sources can smear the response of the weak point source. In the *Einstein* observations (Watson *et al.* 1981), Sgr A West produced an X-ray flux about one-seventh that of A1742−294 and twice that of 1E 1743.1−2843. If Sgr A West had a persistent X-ray flux corresponding with this ratio during our observations, we should have detected it as a point source. Allowing for the possibility that the interference from other sources in our scan-produced *image* is nonuniform, enabling us to see 1E 1743.1−2843 but not Sgr A West, the model fitting can be used to set a 3 σ upper limit to the intensity of Sgr A West at 2.0 count s^{-1} for 660 cm^2 (the Table 2 value) in the 2–10 keV band, or $\sim$1 UFU, which is less than half the intensity of 1E 1743.1−2843. We therefore consider the following possibilities to be more likely than interference from more intense sources: (1) this source is variable on a long time scale, and it was in a low state (less than 25% of its 1979 intensity) during the observations of Spartan 1. Alternatively, the X-ray source at Sgr A West has not changed since the *Einstein* observations, but (2) because it has a soft energy spectrum, it is below the detection threshold of our observations, or (3) its intensity is variable on a time scale comparable to, or larger than the passage time of the collimator, so that it did not appear as a steady point source. However, the Galactic center X-ray point source was labeled as "hard" in Watson *et al.* (1981), rendering possibility (2) unlikely. On the other hand, since most X-ray sources are known to be variable over a broad range of time scales, possibilities (1) and (3) remain plausible. If a relationship existed between the 511 keV gamma-rays associated with a source at the Galactic center (Leventhal and McCallum 1982; Ramaty and Lingenfelter 1986) and the X-ray source, then the turn-off of the gamma-ray emission in 1980 may have been coincident with an X-ray turn-off. This lends support to the idea that a 511 keV source is associated with Sgr A West (Leventhal 1987).

b) *The Number of Sources Detected*

While 12 point sources within 1° of the Galactic center were derived from the *Einstein* observations (Watson *et al.* 1981), the Spartan 1 experiment detected only six point sources in the same region. Two sources in the *Einstein* observations were labeled as "soft," and perhaps could not have been detected by Spartan 1. The remaining sources, which we did not detect, are distributed mostly in a small region with a separation of a few arcminutes. Since the narrow width of the Spartan 1 collimator is 5′ and the mean resolution achieved on the MEM map is 3′, it is difficult to resolve weak sources clustered in such a small region. These sources are likely to have been observed as part of the central diffuse component. However, as noted earlier, the *Einstein* map showed a region of prominent emission (sources 11 and 12; Watson *et al.* 1981) which was detected neither in our MEM map nor by the fitting technique. Therefore some of the X-ray sources within 1° of the galactic center, in addition to Sgr A West and SP 1744.2−2959, may be variable over time scales of a few years.

c) *Diffuse Components*

We detected two diffuse components which differ in their energy spectra: a centrally located diffuse emission with a relatively high absorption, and a uniform background emission with little absorption. In addition to its close proximity to the Galactic center, the centrally located diffuse component also has an absorption column density consistent with a location at the Galactic center (see Fig. 3). We therefore consider it to be a disk-shaped region at the Galactic center, with a radius of $\sim$100 pc and half thickness of $\sim$40 pc. Its total luminosity $\approx 4 \times 10^{36}$ ergs s^{-1} in the energy range 2–10 keV agrees well with the luminosity of the diffuse component observed by Watson *et al.* (1981), which is 2.2×10^{36} ergs s^{-1} in the 0.9–4.0 keV band. We cannot exclude the possibility that some of the weak point sources in the *Einstein* observations contributed to our central diffuse component, although their contribution is probably less than 10% of the diffuse luminosity. Watson *et al.* (1981), discussing whether it is truly diffuse in nature or merely a collection of point sources, showed how difficult it was to generate the diffuse emission by three elementary processes: synchrotron radiation, inverse Compton scattering, and thermal bremsstrahlung. Our central diffuse component is essentially consistent with the *Einstein* result, and we agree with their conclusion that the diffuse source is unlikely to be truly diffuse, and instead is a collection of unresolved point sources. We can set an upper limit to their luminosity of 4×10^{34} ergs s^{-1} each, and a lower limit of 100 to the number of sources to explain the central diffuse component; however, this constraint is much less stringent than that derived from the *Einstein* observations. In addition to the low-luminosity stellar sources discussed by Watson *et al.* (i.e., OB and T Tauri stars), we cannot reject the possibility that these sources could be Be star binaries like γ Cas or X Per, or white dwarf binaries (Hertz and Grindlay 1984).

For the uniform background, we need at least two components to fit the pulse height spectrum. One of the models we employed to fit the spectrum was a combination of a thermal bremsstrahlung and a power-law component. The thermal component represents the emission in the lower energy range 1–5 keV, while the power-law component represents that in the higher energy range, 5–10 keV. The latter might contain some contribution from the intrinsic particle background. The best-fit temperature for the thermal component is ~ 3 keV with absorption column density $N_H \approx 4 \times 10^{21}$. The surface intensity is $\sim 2 \times 10^{-7}$ ergs s^{-1} cm^{-2} sr^{-1} in the energy range 2–10 keV (or ~ 20 counts cm^{-2} s^{-1} sr^{-1}).

This uniform component has a strong similarity to the diffuse X-ray emission from the Galactic ridge observed by *HEAO 1* (Worrall *et al.* 1982), *EXOSAT* (Warwick *et al.* 1985), and *Tenma* (Koyama *et al.* 1986). The *HEAO 1* observations were made only at high longitude ($|l| > 50°$), and probably are not appropriate for comparison with our Galactic center results. The *EXOSAT* observations, though contaminated by a large number of point sources, cover the region including the Galactic center and allow us to estimate the surface intensity there fairly accurately. The *Tenma* observation was conducted at medium longitude ($l \approx 330°$) and detected strong line emission from ionized iron with excellent spectral resolution. The emission from the Galactic ridge detected by these observations is the most likely explanation of the uniform background detected by Spartan 1, at least for the low-energy component. The surface luminosity of our low-energy component is similar to that observed by *EXOSAT* (1.8×10^{-7} ergs s^{-1} cm^{-2} sr^{-1} in the energy range 2–6 keV) and *Tenma* (0.8×10^{-7} ergs s^{-1} cm^{-2} sr^{-1} in the energy range 2–10 keV). The spectral temperature (3 keV) is somewhat lower than that derived by *EXOSAT* (~ 6 keV) and *Tenma* (~ 5 to 10 keV, varying with sky position), but consistency might be achieved by considering the higher energy, power-law component. The absorption column density of $N_H \approx 4 \times 10^{21}$ is lower than that of most of the point sources near the Galactic center. This is the first measurement of the spectrum of this "uniform" diffuse emission, and it suggests that the source of emission is some extended region lying in the galactic plane between the solar system and the galactic center. The *EXOSAT* observations claim that the scale height of the emission in the galactic plane to be 100 pc, which corresponds to about 0°.5 at the Galactic center. This is the only major inconsistency between Spartan 1 and other observations, since we derived the uniform background on the assumption that it is flat over a region 3° from the Galactic center. Our coverage, however, was low in the outer part of this region both in observation time and collimator response, and we cannot deduce a scale height. Therefore we conclude that we detected the X-ray emission from the Galactic ridge as a low-temperature component of the uniform background in the Galactic center region.

V. SUMMARY AND CONCLUSIONS

Spartan 1 observed four strong, point X-ray sources near the galactic center: A1742−294, 1E 1740.7−2942, 1E 1743.1−2843, and the new source, SP 1744.2−2959, $\sim$0°.5 southeast of A1742−294 (see Fig. 1). GX 3+1 was observed on the collimator edge during six scans. The spectral parameters of A1742−294, GX 3+1, and SP 1744.2−2959 are virtually identical (see Fig. 3). Because GX 3+1 is a QPO source (Lewin *et al.* 1986) and a burster (Inoue *et al.* 1981), and A1742−294 is probably an X-ray burster (Lewin *et al.* 1976), we conclude that SP 1744.2−2959 probably belongs to the same class as QPO or burst sources. The remaining two sources, 1E 1740.7−2942 and 1E 1743.1−2843, show relatively hard spectra and (probably intrinsic) high absorption, not unlike GX 301−2 (White and Swank 1984; Leahy *et al.* 1987) and thus could be binary X-ray pulsars, although this is not required.

Instead of a hard X-ray point source at the poition of Sgr A West, Spartan 1 detected hard X-ray diffuse emission, centered near Sgr A West, $\sim 1°$ in extent along an axis aligned to within 20° of the Galactic equator, with a maximum (2–10 keV) surface intensity of $\sim 1.5 \times 10^{-6}$ ergs cm^{-2} sr^{-1}. The spectrum of the centrally localized diffuse emission is similar to those of the strong, galactic center sources, A1742−294, GX 3+1, and SP 1744.2−2959 (see Fig. 3). The hard X-ray point source at the Galactic center was at least 4 times weaker during the 1985 Spartan 1 observations than it was during the 1979 *Einstein* observations (Watson *et al.* 1981—see § IV*a*).

There is also evidence from Spartan 1 for two, weaker point X-ray sources embedded in the centrally localized diffuse emission, located $\sim$0°.1 northeast and southeast of Sgr A West (GC NE and GC SE—see Fig. 2). Only the GC NE source is resolved in the MEM map. GC SE is the only source detected by Spartan 1 which could be considered soft, the only nearby *Einstein* source is hard (5—Watson *et al.*). If its spectrum were not attenuated below 2 keV by intrinsic self-absorption, then GC SE would be a very bright source (see Table 2), giving it the characteristics of a class of black hole candidates.

Finally, there is an additional uniform diffuse emission which appears to persist over the central 2°.5 around the Galactic center. This uniform emission has an intensity of $\sim 2 \times 10^{-7}$ ergs cm^{-2} s^{-1} sr^{-1}, weaker than the centrally localized diffuse emission by almost an order of magnitude, and having a hard spectrum lacking the high column absorption evident in spectra of the other galactic center sources. This uniform diffuse emission may be an extension of the Galactic ridge emission observed by *HEAO 1*, *EXOSAT*, and *Tenma*, but not all of its characteristics are consistent with this source (see § IV*c*).

We would like to acknowledge the consistent and generous support of the High-Energy Astrophysics office at NASA Headquarters, as well as the backing of the authors' home institutions (LANL, NRL, and Northwestern University). The work at Los Alamos was performed under the auspices of the US Department of Energy, and financial support to NRL was provided by NASA NDPR S08096C and S65095B. Our sincere thanks to go the the many engineers and technicians, under the leadership of David J. Shrewsberry, of the Special Payloads

Division at GSFC, for the enthusiasm and skill they brought to the construction and flight of Spartan 1.

We would like to thank also the engineers at KSC, in particular Dean Zimmermann, who integrated Spartan 1 into Discovery with great efficiency, and to the team at JSC who developed and carried out the Spartan 1 flight operations, including Wayne Eaton (Payload Integration Manager, NASA), Gary Gutschewski (Spartan Payload Officer, NASA), J. Milton Heflin (Flight Director, NASA), Craig Gross (Rendezvous Engineer, McDonnell Douglas), and last, but most, the shuttle crew, Cdr. Daniel C. Brandenstein, Cdr. John O. Creighton (USN), Col. John M. Fabian (USAF), Dr. Shannon W. Lucid, and Col. Steven R. Nagel (USAF).

Many people contributed to the preparation of the experiment, but special mention is due to Richard Blake, Harry Felthauser, and Ernie Serna (LANL), Robert Tait, Donald Woods, and Michael Kowalski (NRL). The Spartan 1 software has benefited from the diligent efforts of Kevin Carmody (NRL), and Joseph Greene, Joseph Hora, Steven Majewski, and James Pendleton (NU). We would also like to thank Margaret Hamilton of NRL for her indispensible administrative support of Spartan 1.

APPENDIX

I. GENERATION OF THE MEM MAP

The object of the MEM technique is to produce the most probable image consistent with the data. In practice this involves trading the smallest possible reductions of the image entropy for given reductions in χ^2. The entropy was defined as $-\Sigma b_i \ln (b_i)$, where b_i is the intensity of the ith map pixel. To accomplish this we performed three different types of iterations in the construction of the MEM image.

The MEM image was generated by first using the iterations described in Willingale (1981) which estimate the logarithm of the lattice point intensities for the next iteration of the map using the product of a Lagrange multiplier and the residuals. The residuals are calculated by first taking the difference between (*a*) the convolution of the collimator response with the lattice intensities of the current map; and (*b*) the corresponding data sample. The residuals are then formed by dividing the *negative* of the differences by the square of the corresponding data point error, and then convolving again with the collimator response (this time for a fixed *field* position). No pixel of the estimated map was allowed to exceed the value of the previous map by more than a factor of e (2.718...). Each new map was generated using 33% of the estimated map and 67% of the current map. During the first few iterations the entropy *increased* with decreasing χ^2, which implied the method was working well. In addition, as long as the interations generated maps whose predicted data counts were increasingly large *fractions* of the actual data counts, the maps were not scaled to the data counts. However, the entropy always was calculated as if the map were scaled so that the predicted (map) counts were equal to the actual counts. Once the map started to fall short of those of the previous map, then the maps were scaled between iterations. When χ^2 reached about 10,500 for the 8657 data points (the data from detectors 1 and 2 were treated separately), the entropy started to *decrease* with decreasing χ^2. At this point, we changed the iterative technique, using the Newton-Raphson method (between scaling iterations) to search for a zero of the residual of *each* lattice point, by adjusting the corresponding logarithmic map intensities at the independent variable. The equation for logarithm of the new map is then given by:

$$\ln b^{i+1}{}_{k1} = \ln b^{i}{}_{kl} - \mathrm{Res}^{i}{}_{kl} * \ln (b^{i}/b^{i-l})/(\mathrm{Res}^{i}{}_{kl} - \mathrm{Res}^{i-l}{}_{kl}) \tag{1}$$

where $b^{i-1}{}_{kl}$, $b^{i}{}_{kl}$, and $b^i + 1_{kl}$ are the intensities of the klth lattice point for the $(i-1)$th, ith, and $(i+1)$th iterations, respectively; b^i/b^{i-1} is the scaling factor (independent of kl) used to generate the (scaled) ith map from the $(i-1)$th map; and Res_{kl} represents the residual of the klth lattice point. The step size for $\ln (b_{kl})$ for the Newton's method defined by equation (1) is conservatively small, in that the (smaller) residuals of the scaled ith map are used to represent the value of the dependent variable, rather than the mean of the residuals of the scaled *and* unscaled maps, $0.5 * [(i-1)\text{th} + i\text{th}]$, which would always be larger in absolute value. Again, no pixel was allowed to grow by more than e during the iterations defined by equation (1). Once the $(i+1)$th map was scaled to the data, forming the $(i+2)$d map, this method reduced χ^2 more per given loss of entropy than the continuation of the Lagrange multiplier method described above. In this manner, χ^2 was reduced from 10,500 to 9200 while the entropy decreased by a factor of 0.92. By this time, the fractional decrease of the χ^2 per iteration was between 0.5 and 1.0 of the fractional loss in entropy, so that little further reduction in χ^2 could be achieved without unacceptably large sacrifices of entropy. At this point the iterative technique was again changed, using the following expression for the intensity:

$$b^{i+1}{}_{kl} = b^{i}{}_{kl}/\exp\,[1. - 1/(2. + \ln (b^{i}{}_{kl})] \, . \tag{2}$$

This is the explicit Newton-Raphson method of iteration to find a null in the derivative of the entropy with respect to $\ln (b_{kl})$ (the Lagrange multiplier is set to zero). Each of the iterations defined by equation (2) was followed by a scaling iteration, as was done for the Newton's method employed previously. These pairs of iterations increased the entropy while (at first) decreasing χ^2. Soon, however, a minimum of χ^2 was reached, and the iterations were stopped. Simulations with larger bodies of data with more complete scan coverage have shown that this method can also be very useful for nonzero values of the Lagrange multiplier (see below, and also Cornwell and Evans 1985).

The map generated by using these three techniques did not differ qualitatively from that generated by using only the first (i.e., Willingale's) method but yielded point source intensities which, for the most part, were generally higher (although the intensity integrated over the point source is constrained to remain constant by the χ^2). The final map fitted the data with a χ^2 of 9114.83 for 8657 data points, with 28,976 counts above the uniform diffuse background, and an entropy of -3.42842×10^7, on a lattice with 58,081 nodes.

Further reduction of the χ^2 was possible by using an iteration such as:

$$b^{i+1}{}_{kl} = b^{i}{}_{kl} * \exp \{[-1. - \ln (b^{i}{}_{kl}) + \lambda * \mathrm{Res}^{i}{}_{kl}]/[2. + \ln (b^{i}{}_{kl}) - \lambda * \mathrm{Res}^{i}{}_{kl}]\} . \tag{3}$$

By using these iterations with $\lambda = 10.$ at first, then decreasing to ~ 0.5 or 0.25, then interrupting with one iteration as described by equation (1) before making additional iterations as in equation (3), we were able to produce a map with a $\chi^2 = 8728.71$ and an entropy of -3.47282×10^7, a 4.2% drop in χ^2 for only a 1.3% sacrifice in entropy. In this map, the local maximum between sources 2 and 3 becomes more ridge like, with *Einstein* sources 2 and 3 both definitely on the opposite sides of the ridge. This map also showed an extra source with a peak brightness of ~ 640 counts s^{-1} cm^{-2} sr^{-1} at right ascension $17^{\mathrm{h}}41^{\mathrm{m}}.75$ and declination $-28°.574$. This source lies on the line of artifacts seen leading to GX 3+1 in the maps generated before GX 3+1 was subtracted from the data. Thus it is probably an artifact resulting from either the poorly simulated wide response of the collimator, or time variability of GX 3+1, or both, Moreover, the linear fitting technique assigned only 0.3–0.5 counts s^{-1} to this source, with a drop in χ^2 of only 3–4 for the extra three parameters used. Thus we chose not to use this revised map in our Figures 1 and 2 due to the unverifiable nature of the additional source.

II. ADDITIONAL SIMULATIONS

We also simulated data using the parameters for the linear fitting solution for the seven point sources and the centrally localized diffuse emission. We then generated a map from this simulated data using the iterations described by Willingale (1981) and then those of equation (1). Very little gain was achieved by using the iterations of equation (3). This map was extremely similar to the map derived from the real data shown in Figure 2, with a local maximum just west of the linear fitted position for source 10, a narrow saddle just west of *Einstein* source 9, another local maximum between GC NE and *Einstein* source 6, and a southern extension west of GC SE. However, although the contours do extend toward *Einstein* source 10 from the local maximum before dropping precipitously to the east, the effect is much less abrupt than that shown in Figure 2, the contours of the map of the simulated data being much more circular. Also unlike the map generated from the real data, the χ^2 of the map from the simulated data was easily decreased to 8261, with an entropy of -3.65743×10^7. The χ^2 of the simulated data tested against the model map fell in the upper 7900's. The decrepancy between these lower χ^2 values and the higher values associated with the MEM map derived from, and the linear fit to, the real data was due to using the data counts to estimate the error, rather than the counts estimated from the *convolution of the collimator with the map*, which are smaller for the predominance of regions with low map intensity.

In an effort to increase the map intensity in the otherwise "blank" regions near the centrally localized diffuse emission we defined the χ^2 using the counts derived from the map intensities instead (but ignored the explicit dependence of χ^2 on this intensity in the reciprocal square of the errors when taking the derivative to define the residual). The χ^2 of this map settled to 8987 with an entropy of -3.65747×10^7 when the iterations were exhausted. Again, unlike the iterations of the real data, little gain was achieved by using the iterations described in equation (3). This map lacked the southern extension to the west of GC SE present in the previously simulated map and to some degree in the real data maps, having instead a similar southern extension to the *east* of GC SE. The map also had no contours covering Sgr A West down to a level of 365 counts s^{-1} cm^{-2} sr^{-1} with only a small loop of the 400 counts s^{-1} cm^{-2} sr^{-1} contour covering source 2 and extending 3′ to the south. The GX 3+1 artifact near $17^{\mathrm{h}}41^{\mathrm{m}}$, 28°.574 rises to over 860.7 counts s^{-1} cm^{-2} sr^{-1}; three other artifacts of slightly smaller maximum brightness appear in the map near the western border of the $e^{-1/2}$ contour of the centrally localized diffuse emission.

Finally, in order to test the sensitivity of the map to the location of the point sources, we also produced a map from data simulated with the northern source located at *Einstein* source 10, and GC NE at *Einstein* source 6. This map differed drastically from the previous maps. The local maximum near source 10 fell on the position derived from the linear fitting (to the real data), with the contours dropping steeply to the east before rising again to a local maximum $\sim 5'$ east of source 10, but dropping only gradually for a circular region extending 5′ to the west. A narrow saddle does occur just west of source 9, but jumps abruptly to a local maximum around source 6 (the abrupt shoulders lying on the north and northwest sides of this source), before dropping steeply, but not abruptly, to the east and south. A saddle forms south of the GC NE position which rises gradually to a local maximum about 4′ west-southwest of GC SE. This new local maximum then drops abruptly along its eastern, southern, and western borders.

Because the linear fitting and the MEM map iteration process are affected by the same systematics, we cannot use this example to say that our north source is distinct from *Einstein* source 10, or that GC NE differs from *Einstein* source 6. We can say, however, that the MEM map and the linear fitting solution are as consistent with each other as possible.

REFERENCES

Bradt, H. V., Doxsey, R. E., and Jernigan, J. G. 1979, *Adv. Space Exploration*, **3**, 17.

Bradt, H. V., and McClintock, J. E. 1983, *Ann. Rev. Astr. Ap.*, **21**, 13.

Branduardi, G., Ives, J. C., Sanford, P. W., Brinkman, A. C., and Maraschi, L. 1976, *M.N.R.A.S.*, **175**, 47P.

Cornwell, T. J., and Evans, K. F. 1985, *Astr. Ap.*, **143**, 77.

Cruddace, R. G., Fritz, G., Shulman, S., Friedman, H., McKee, J., and Johnson, M. 1978, *Ap. J. (Letters)*, **222**, L95.

Czerny, B., Czerny, M., and Grindlay, J. E. 1986, *Ap. J.*, **311**, 241.

Eyles, C. J., Skinner, G. K., and Willmore, A. P. 1975, *Nature*, **257**, 291.

Fritz, G. G., *et al.* 1987, in preparation.

Gull, S. F., and Daniel, G. J. 1978, *Nature*, **272**, 636.

Hertz, P., and Grindlay, J. E. 1984, *Ap. J.*, **278**, 137.

Inoue, H., *et al.* 1981, *Ap. J. (Letters)* **247**, L23.

Jernigan, J. G., Apparao, K. M. V., Bradt, H. V., Doxsey, R. E., Dower, R. G., and McClintock, J. E. 1978, *Nature*, **272**, 701.

Kellogg, E., Gursky, H., Murray, S., Tananbaum, H., and Giacconi, R. 1971, *Ap. J. (Letters)*, **169**, L99.

Koyama, K., Makishima, K., Tanaka Y., and Tsunemi, H. 1986, *Pub. Astr. Soc. Japan*, **38**, 121.

Leahy, D. A., Nakajo, M., Matsuoka, M., Kawai, N., Koyama, K., and Makino, F. 1987, *Pub. Astr. Soc. Japan*, submitted.

Leventhal, M. 1987, in *Proc. of the 13th Texas Symposium on Relativistic Astrophysics*, ed. M. P. Ulmer (Singapore: World Scientific Publishing Corp.), p. 382.

Leventhal, M., and McCallum, C. J. 1982, in *AIP Conference on the Galactic Center*, ed. G. R. Reigler and R. D. Blandford (New York: AIP), p. 132.

Lewin, W. H. G., *et al.* 1976, *M.N.R.A.S.*, **177**, 83P.

Lewin, W. H. G., *et al.* 1986, *M.N.R.A.S.*, submitted.

Makishima, K., *et al.* 1986, *Ap. J.*, **308**, 635.

Mitsuda, K., *et al.* 1984, *Pub. Astr., Soc. Japan*, **36**, 741.

Ohashi, T., *et al.* 1984, *Pub. Astr., Soc. Japan*, **36**, 699.

Press, W. H., Flannery, B. P., Teukolsky, S. A., and Vetterling, W. T. 1986, *Numerical Recipes* (Cambridge: Cambridge University Press) p. 468.
Proctor, R. J., Skinner, G. K., and Willmore, A. P. 1978, *M.N.R.A.S.*, **185**, 745.
Ramaty, R., and Lingenfelter, R. E. 1986, *Ann. NY Acad. Sci.*, **470**, 215.
Warwick, R. S., Turner, M. J. L., Watson, M. G., and Willingale, R. 1985, *Nature*, **317**, 218.
Watson, M. G., Willingale, R., Grindlay, J. E., and Hertz, P. 1981, *Ap. J.*, **250**, 142.
White, N. E., Kaluzienski, L., and Swank, J. H. 1984, in *Proc. AIP Conference on High Energy Transients in Astrophysics*, ed. S. E. Woosley (New York: AIP), p. 31.
White, N. E., and Marshall, F. E. 1984, *Ap. J.*, **281**, 354.
White, N. E., and Swank, J. H. 1984, *Ap. J.*, **287**, 856.
White, N. E., Swank, J. H., and Holt, S. S. 1983, *Ap. J.*, **270**, 711.
Willingale, R. 1981, *M.N.R.A.S.*, **194**, 359.
Wilson, A. M., Carpenter, G. F., Eyles, C. J., Skinner, G. K., and Wilmore, A. P. 1977, *Ap. J.* (*Letters*), **215**, L111.
Worrall, D. M., Marshall, F E., Boldt, E. A., and Swank, J. H. 1982, *Ap. J.*, **255**, 111.

R. G. Cruddace, G. G. Fritz, and W. A. Snyder: Space Science Division, Code 4120; Naval Research Laboratory, Washington, DC 20375

E. E. Fenimore and J. Middleditch: ESS-9, MS D436, Los Alamos National Laboratory, Los Alamos, NM 87545

N. Kawai: Cosmic Ray Laboratory, The Institute of Physical and Chemical Research (RIKEN), Hirosawa 2-1, Wako-shi, Saitama, 351-01 Japan

M. P. Ulmer: Department of Physics and Astronomy, Northwestern University, Technological Institute, Evanston, IL 60201